

A&A manuscript no.

(will be inserted by hand later)

Your thesaurus codes are:

3(11.17.3; 12.12.1; 13.25.3; 01.13.2; 12.04.2)

ASTRONOMY
AND
ASTROPHYSICS

The large-scale diffuse X-ray emission surrounding quasars: an investigation using the scaling-index method

K. A. Williams*, W. Brinkmann, and G. Wiedenmann

Max-Planck-Institut für extraterrestrische Physik, Giessenbachstrasse, D-85740 Garching, FRG

Received ? / Accepted ?

Abstract. The large-scale ($\sim 20'$) diffuse x-ray background surrounding a sample of quasars observed during *ROSAT* PSPC pointed observations is studied using a new source-detection algorithm, the scaling-index method. This algorithm, which can identify individual photons as belonging to a source or background, is useful for detecting faint, extended sources in noisy fields. Using this method, we find that, contrary to conclusions drawn by others, there is scant evidence for preferential enhancement of x-ray backgrounds surrounding radio-loud quasars by foreground x-ray emitting clusters of galaxies. Rather, all fluctuations in these backgrounds can be explained by varying levels of emission from a galactic thermal plasma of temperature $T \approx 0.14$ keV. No difference is observed between the diffuse x-ray backgrounds of radio-loud and radio-quiet quasars.

Key words: quasars: general – large-scale structure of Universe – X-rays: general – Methods: data analysis – diffuse radiation

1. Introduction

It is generally agreed that radio-loud quasars and radio-quiet quasars reside in markedly different environments for redshifts $z \gtrsim 0.6$, with radio-loud quasars lying in rich clusters and radio-quiet quasars residing in smaller clusters (Boyle 1988), although some evidence has been introduced to the contrary (Fried 1997). Burg et al. (1994) and Briel & Henry (1993) have shown that rich clusters, namely, Abell clusters, are luminous x-ray sources and that the cluster richness is correlated with the x-ray luminosity. Naïvely combining these two results leads to the conclusion that the background x-ray emission surrounding radio-loud quasars should be higher than the background emission surrounding radio-quiet quasars.

Unfortunately, the expected evolution of clusters with time does not permit us to make such a straightforward conclusion. Hall et al. (1995) summarize arguments where, depending upon the model used to explain the associations of radio-loud quasars with richer host clusters, the x-ray luminosity of the host cluster may be weaker than expected, especially if the host clusters are not virialized. The search of Hall et al. for x-ray emission from the host clusters of two moderate-redshift quasars failed to find any such emission. This result suggests that the direct detection of x-ray emission from quasar host clusters would be very difficult.

Bartelmann et al. (1994, hereafter BSH) searched for diffuse x-ray emission around radio-loud quasars using *ROSAT All-Sky Survey* (RASS) data. They claim to have found significant detections of diffuse emission on angular scales of $\gtrsim 10'$ for distant ($z \gtrsim 1.5$) and nearby ($z \lesssim 1.0$) radio-loud quasars, while radio-loud quasars with intermediate distances displayed no significant excess diffuse emission. They argue that the sources of the excess emission surrounding the distant quasars are most likely foreground clusters of galaxies, themselves diffuse x-ray emitters. They estimate an excess count rate on the order of 10^{-2} s^{-1} in the RASS due to these hypothetical clusters.

In order to study further the correlation of quasars with x-ray emission and in order to compare the diffuse x-ray backgrounds surrounding radio-loud and radio-quiet quasars, we undertook a comparison study of the x-ray backgrounds surrounding quasars observed with the *ROSAT* Position-Sensitive Proportional Counter (PSPC) (Pfeffermann et al. 1980) during the pointed-observation mode of the mission. The main advantage of the pointed observations over the RASS observations is a large increase in sensitivity. The typical observing time for RASS fields near the ecliptic plane is 400 sec (Voges et al. 1996), while the pointed observations discussed here had net exposure times of ≥ 10 ksec. Such an observing time also should permit us to detect the hypothetical clusters of BSH. The pointed observations also have a higher angular resolution, which aids in source detection. One disadvantage to the use of pointed observations is the selection effect introduced by the pointed observations themselves;

Send offprint requests to: K. Williams (williams@ucolick.org)

* Present address: UCO/Lick Observatory and Board of Astronomy and Astrophysics, University of California, Santa Cruz, CA 95064, USA

presumably, mainly “interesting” objects were targeted by the initial observer. This introduces unknown and unquantifiable biases into our quasar sample.

Additionally, the work of BSH compared backgrounds surrounding radio-loud quasars to “blank” fields. In this study, we compared the radio-loud quasar backgrounds to radio-quiet quasar backgrounds rather than blank fields. According to McHardy et al. (1998), deep *ROSAT* images result in a surface density of QSOs of $129 \pm 28 \text{ deg}^{-2}$ for R-band magnitudes brighter than 21. For our fields, this would imply around 45 QSOs in each field. Even if only a small fraction of these were detectable in a 10 ksec exposure, the search for control fields devoid of QSOs would be formidable.

2. Data Analysis

2.1. Sample Selection

The sample consists of quasars from the catalogue of Véron-Cetty & Véron (1993) viewed during *ROSAT* PSPC pointed observations, either as targeted or serendipitously-observed objects. All selected observations are available in the public *ROSAT* data archive. This list contains 127 quasars, of which 27 have been detected in the radio band.

In order to obtain a uniform sample, we selected 10 050 seconds of observing time from each PSPC observation in twenty-five 402-second intervals, each interval corresponding to the wobble period of the *ROSAT* spacecraft. The particle background was minimized by selecting only those intervals where the Master Veto Rate was between 40 and 170 counts s^{-1} and the oxygen column density was less than $1.0 \times 10^{15} \text{ cm}^{-2}$. Further contamination was removed by examining the accepted and transmitted count rate and rejecting time intervals where this rate was markedly above the average, which varies depending on the total flux of the targeted field. We minimized the contamination of the extragalactic background from galactic emission by selecting only those events with an amplitude > 60 , corresponding to photon energies $\gtrsim 0.6 \text{ keV}$. We rejected fields where the candidate quasar was located outside the central $20'$ of the PSPC field of view in order to minimize vignetting and off-axis image degradation. These selection criteria resulted in the reduction of the sample to 72 quasars.

The sample size was further reduced by rejecting fields where the quasar was not detected by the scaling index method (Wiedenmann et al. 1997, hereafter WSV, see §2.2). We rejected four additional fields, containing a total of five quasars, due to their location in areas of extended galactic hard x-ray emission such as Loop I. One quasar near the x-ray bright galaxy cluster Abell 1795 was rejected due to the large angular extent of the cluster, which introduced very large uncertainties in the background corrections. Two further fields containing one sample quasar

each were rejected due to anomalous light curves of the observed background (variations greater than 2σ in the observed count rate).

The remaining 33 quasars constituting the sample used in our analyses are listed in Tab. 1. The table includes the names and redshifts of the objects as listed in Véron-Cetty & Véron. The listed coordinates are precessed to J2000.0 from the coordinates in the catalogue. The start-of-observation dates for each image (in *ROSAT* days) is provided, as is the adopted neutral hydrogen value for each quasar (see §2.3). Columns then list the total number of background photons in the accepted fields as measured from both the maximum-likelihood and scaling-index method algorithms described below. Next, the detected photon fluxes in photons $\text{sec}^{-1} \text{ deg}^{-2}$ are listed. We did not attempt to unfold the events through the PSPC detector response matrix.

As previously mentioned, these fields were imaged during *ROSAT* PSPC pointed observations. In such observations, structures in the image caused by the filter support struts are visible in each image. In order to remove these structures from the analysis, we selected only those photon events located within a $20'$ radius of the detector center.

2.2. The Scaling Index Method

Suppose we have observed N photons (x_1, \dots, x_N) within a PSPC image. This map is described by the set $\{d_{ij}\}$ of distances between all photons. For each of the N photons the cumulative number function is calculated

$$N_i(r) = \# \{j | d_{ij} \leq r\}, \quad (1)$$

where $\#\{j\}$ means the total number of elements in the set $\{j\}$. We approximate the function $N_i(r)$ for each i in some given range $[r_1, r_2]$ with a power law $N_i(r) \sim r^{\alpha_i}$ ($r_1 < r < r_2$) and call the α_i “scaling indices” (or “crowding indices” as introduced by Grassberger 1988). Explicitly, the α_i are given by

$$\alpha_i = \frac{\log N_i(r_1) - \log N_i(r_2)}{(\log r_1 - \log r_2)}. \quad (2)$$

The possible values of the scaling indices for a given scaling range $[r_1, r_2]$ are determined by the conditional probability to find n_2 objects in a ball of radius r_2 , if a ball with the smaller radius r_1 contains n_1 objects. For a given scaling range $[r_1, r_2]$ only those values of α_i will be observed for which two natural numbers n_1, n_2 exist, such that

$$\alpha_i = \frac{\log n_1 - \log n_2}{2(\log r_1 - \log r_2)} \quad (3)$$

and

$$\text{Prob}(N_i(r_2) = n_2 | N_i(r_1) = n_1) > 0. \quad (4)$$

The latter conditional probability depends on the process that produced the observed photon map.

Table 1. Quasar sample after defined selection process. The horizontal line separates radio-quiet QSOs from radio-loud QSOs (above and below line, respectively)

Name	RA (<i>J</i> 2000)	Dec (<i>J</i> 2000)	<i>z</i>	Date of Obs. ^(a)	N_H (10^{20} cm ⁻²)	N_{ML} ^(b)	N_{SIM} ^(b)	Φ_{SIM} ^(c)
E 0015+162	0 18 31.9	16 29 26	0.554	782.2	4.07	2701.6	2762.1	0.7470
PHL 6625	0 46 51.8	-20 43 30	0.380	576.1	1.57	2511.1	2652.6	0.7174
SGP 2:20	0 51 52.9	-29 15 00	0.601	742.3	1.80	2531.8	2685.1	0.7262
SGP 3:19	0 54 59.1	-28 14 30	0.779	590.4	1.80	2531.6	2717.0	0.7348
SGP 3:39	0 55 43.3	-28 24 09	1.964	590.4	1.89	2540.4	2724.5	0.7368
SGP 4:41	0 57 24.5	-27 31 60	1.209	774.2	1.86	2142.2	2375.6	0.6425
E 0121+034	1 24 33.2	3 43 35	0.336	788.0	3.37	2503.0	2555.0	0.6910
NGC 520.40	1 24 57.5	3 53 48	1.205	788.0	3.27	2493.4	2547.4	0.6889
Q 0123-005B	1 26 02.2	-0 19 24	1.761	788.0	3.36	2057.2	2263.8	0.6122
MS 02074-1016	2 09 56.8	-10 02 51	1.970	602.1	2.22	2329.3	2453.1	0.6634
QSF 3:31	3 41 55.8	-44 16 37	1.797	1177.2	1.66	2065.8	2295.2	0.6207
PG 1115+080	11 18 17.0	7 45 60	1.722	550.7	3.62	2555.8	2578.9	0.6974
PG 1116+215	11 19 08.7	21 19 18	0.177	367.1	1.40	2707.7	3003.2	0.8121
US 2694	11 36 55.0	29 51 32	1.858	368.1	1.77	2417.6	2735.6	0.7398
PG 1411+442	14 13 48.3	44 00 14	0.089	396.2	1.05	2700.6	2874.9	0.7775
QS M5:42	22 02 29.9	-19 01 52	1.045	555.9	2.87	3042.8	3123.4	0.8447
MS 22236-0517	22 26 15.7	-5 02 06	1.866	1103.4	5.08	2568.2	2620.6	0.7087
Mrk 926	23 04 43.4	-8 41 08	0.047	1101.0	3.51	2450.7	2470.3	0.6681
PKS 0122-00	1 25 28.8	-0 05 56	1.070	1155.4	3.29	1987.8	2193.8	0.5933
PKS 0136+176	1 39 41.9	17 53 07	2.716	1157.2	5.02	2270.7	2491.6	0.6738
PHL 1093	1 39 57.2	1 31 47	0.258	1156.4	3.24	2138.0	2353.9	0.6366
3C 208.0	8 53 08.6	13 52 54	1.109	909.6	3.56	2150.4	2351.4	0.6359
3C 212.0	8 58 41.4	14 09 44	1.043	721.3	4.09	2328.1	2491.5	0.6738
3C 216.0	9 09 33.5	42 53 45	0.668	539.0	1.40	2782.2	2996.6	0.8104
4C 54.18	9 10 11.1	54 27 22	0.625	871.2	1.81	1899.5	2032.5	0.5497
B2 0937+39	9 41 04.0	38 53 50	0.618	712.2	1.59	2133.0	2397.7	0.6484
3C 254.0	11 14 38.5	40 37 20	0.734	1098.3	1.97	2317.0	2504.2	0.6772
3C 270.1	12 20 33.9	33 43 12	1.519	1102.9	1.14	1989.8	2210.5	0.5978
PKS 1351-018	13 54 06.8	-2 06 03	3.709	1151.0	3.25	3058.7	3113.7	0.8421
GC 1556+33	15 58 55.1	33 23 18	1.646	423.1	2.44	2962.3	3324.2	0.8990
PG 1718+481	17 19 38.0	48 04 13	1.083	998.2	2.13	2249.4	2468.3	0.6675
3C 446	22 25 47.1	-4 57 01	1.404	1103.4	5.08	2651.5	2693.1	0.7283
3C 454.3	22 53 57.6	16 08 53	0.859	943.2	7.06	3006.8	2935.9	0.7940

(a) ROSAT day, day 0 = 01 June 1990

(b) Corrected total background counts, 10 ksec

(c) photons s⁻¹ deg⁻²

Calculating for all photons x_i the corresponding indices α_i , we get the relative frequency distribution of scaling indices, or scaling index spectrum,

$$N_{freq}(\alpha) = \# \{ \alpha_i | \alpha < \alpha_i < \alpha + \delta\alpha \}. \quad (5)$$

Depending on the random processes in the considered field, $N_{freq}(\alpha)$ has a well-defined envelope and shows gaps, where the probability of equation (4) is zero.

The search for sources or density variations in an otherwise homogeneous and isotropic background is synonymous to the measurement of deviations from the expected frequency distribution. Any inhomogeneity or anisotropy will result either in more power of the frequency distribution at low α -values or in filling up the discrete gaps. Since we have, in general, no precise knowledge about the process producing the background and, as far as we know, no

closed analytical description for $N_{freq}(\alpha)$ exists, another procedure is necessary to separate background photons from source photons.

For different scaling ranges $[r_1, r_2]$ the scaling indices are binned with $\delta\alpha = 10^{-6}$, the computer precision in this case. The r_1 are chosen to be about the size of the expected sources, while $r_2 \approx 10r_1$; in our examples we typically used four different scaling ranges. In a first step, the α -values with $N_{freq}(\alpha) \leq 2$ are singled out for each scaling range. In a second step, only those α -values that have $N_{freq}(\alpha) \leq 2$ in at least two scaling ranges are considered as belonging to source photons. Simulations showed that the number of photons singled out with this procedure in a random Poissonian field are less than 3% of the total number.

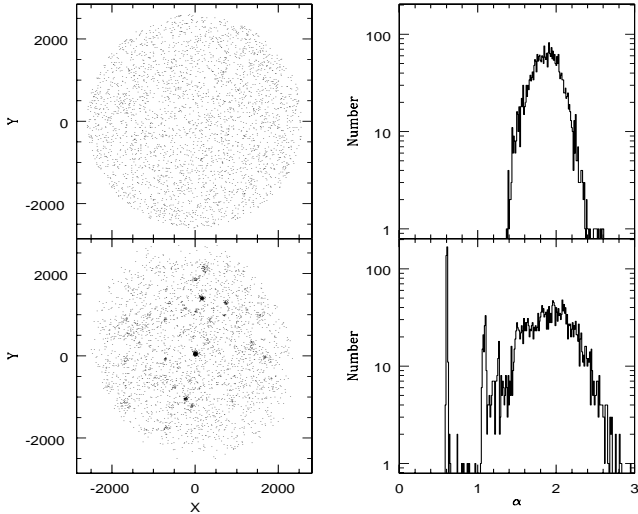


Fig. 1. Photon maps and binned scaling indices α for a randomly-generated, smooth x-ray background (top) and an actual PSPC image of 3C 216 (bottom). The control field contains 3000 randomly-placed photons, a typical background level for the brightest backgrounds in our sample and essentially equivalent to the 1997 photon background of 3C 216. The presence of sources broadens the α distribution, while brighter sources appear as sharp peaks at low scaling index values.

These spurious sources, caused by local fluctuations of the background, can be eliminated by means of a minimal spanning tree (MST) algorithm (Kruskal 1956, Prim 1957), accepting only those sources containing more than a set minimum number of photons. Since we want to find close associations of photons, only those trees of the MST are considered for which all edge-lengths are smaller than a maximally allowed inter-photon separation d_{max} . The value of d_{max} is determined by the mean inter-point separation expected in an isotropic and homogeneous point distribution. This separation is given by $d_{max} \approx \sqrt{A/N}$, where N is the total number of points and A is the area of the region where the N points are found (see WSV 1997).

An example of the scaling-index spectrum is shown in Fig. 1. The upper panels show a randomly-generated, smooth PSPC photon map (left) and the scaling index α -spectrum (right). In an infinite, uniform image, the spectrum would be a delta function located at $\alpha = 2$. Because the field is finite and not infinitely homogeneous, the spectrum is broadened and slightly offset. The lower panels show an actual PSPC image and its α -spectrum. The spikes at low α are the brightest sources, and the peak is broadened further due to the presence of sources.

Analyses of randomly-generated smooth PSPC fields with background levels similar to those in our source fields revealed that the SIM detected spurious sources with source counts up to ~ 5 photons. In order to ensure that

no spurious sources were included in the source lists, we set the lower limit on source counts to ten photons. This limit undoubtedly excluded real sources, but as of yet there is no estimate of source significance available for the SIM.

We applied the SIM algorithm to the fields in this sample, thereby creating source lists and labeling each photon as a source or background photon. Upon removal of the sources, it was obvious that the SIM had not correctly identified all photons, as bright sources remained in the images. Further investigation revealed that the SIM algorithm had difficulty identifying all photons associated with a source if the photon density was very high. We corrected this by identifying all photons within the SIM-defined source boundaries as source photons. We then applied a background correction based on the number of background photons one would expect to find under the source. While this method is less than ideal, the resulting background photon maps appear to have had all detected sources completely removed.

In order to check the effectiveness of the scaling-index method, we also determined the diffuse x-ray background flux of each field using the maximum-likelihood source-detection algorithm included in the *EXSAS* data reduction software package (Zimmermann et al. 1992). Our lower likelihood limit was set at 15, corresponding to a significance level of $\sim 5\sigma$. We set the extraction radius at 2.5 times the FWHM of each source. The background-corrected photon counts were then subtracted from the total photon count to give the raw background photon count. Vignetting corrections were not applied, since we assume that vignetting effects will be similar in each image and since vignetting corrections were not available for the SIM algorithm.

We find that the SIM analysis results in background levels that are higher than the maximum-likelihood technique backgrounds by an average of 158 ± 95 counts. The reason for this discrepancy is not fully clear and should be understood before the SIM is widely implemented. However, part of the discrepancy can be explained by noting that our SIM source flux cut-off of 10 counts, while safely ignoring spurious sources, almost certainly considered numerous true low-flux sources as spurious, resulting in these source photons being treated as background counts.

In this paper, we perform our analysis using the background count levels as calculated by the SIM. A reanalysis of the data using the numbers from the maximum-likelihood technique resulted in the same qualitative conclusions, although the resulting quantities do vary. The SIM analysis has the benefit of identifying each background photon, which made spectral analysis of the background photons straightforward.

2.3. Correction for absorption by neutral hydrogen

Despite our efforts to reduce the effects of absorption by neutral hydrogen, this absorption still affects the observed

background photon counts measurably. The fields in our sample cover a wide range of galactic N_H values, from $1.13 \times 10^{20} \text{ cm}^{-2}$ to $7.06 \times 10^{20} \text{ cm}^{-2}$. We corrected the observed photon counts to a column density of zero. Correction factors were obtained using the most recent *ROSAT* and *ASCA* estimates of the cosmic x-ray background (CXRB) spectrum: a power-law with a photon index of 1.42 and an intensity of $10.0 \text{ keV s}^{-1} \text{ cm}^{-2} \text{ sr}^{-1} \text{ keV}^{-1}$ superimposed on a Raymond-Smith thermal plasma emitting at a temperature of 0.142 keV with an emission measure of 18.8 in XSPEC/EXSAS units per steradian (Miyaji et al. 1998, hereafter Mi98). The lower-temperature thermal plasma component ($T \approx 57 \text{ eV}$) produced by the local hot bubble did not affect our model spectra due to its negligible flux in the observed photon energy band. The model spectrum was then projected through a layer of neutral hydrogen absorption corresponding to the N_H value for each quasar, and the resulting fractional flux decrease due to absorption was added back into the raw background photon count of each field to produce the corrected background counts given in Tab. 1. N_H values were taken from absorption line studies when available (Lockman & Savage 1995; Murphey et al. 1996), otherwise they were calculated from the published HI maps of Dickey & Lockman (1990).

2.4. Spectral Analysis

Taking the background photons as identified by the SIM, we used the *EXSAS* spectral analysis packages to create spectra of the x-ray background in each field. We first attempted to fit the resulting spectrum to the spectrum of Mi98 described above. The goodness-of-fit was checked using a χ^2 test. If the reduced χ^2 indicated a poor fit, we calculated a best-fit spectrum consisting of variable thermal and power-law components.

Example spectra are plotted in Fig. 2. The top spectrum, of the diffuse x-ray background surrounding the radio-loud quasar PKS 0136+176, is fit well by the Mi98 background spectrum (solid line). The lower spectrum is of the diffuse x-ray background surrounding GC 1556+33. The Mi98 spectrum, shown as a dashed line, clearly does not fit the data. The best-fitting spectrum, shown as a solid line, resulted in the same power-law component and thermal plasma temperature as Mi98, only the emission measure of the 0.142 keV thermal plasma was increased. In fact, in virtually every background spectrum a reasonable fit was achieved by varying this emission measure. The best-fit emission measures varied from 15.9 ± 1.7 XSPEC units per steradian for 4C 54.18 to 58.5 ± 2.4 XSPEC units per steradian for GC 1556+33 (Recall the Mi98 spectrum had an emission measure of 18.8 XSPEC units per steradian). This suggests that the variations in diffuse background levels among the fields are due to variations in the hot thermal component of the CXRB, presumed by many to originate in the galactic halo (e.g. Gendreau et

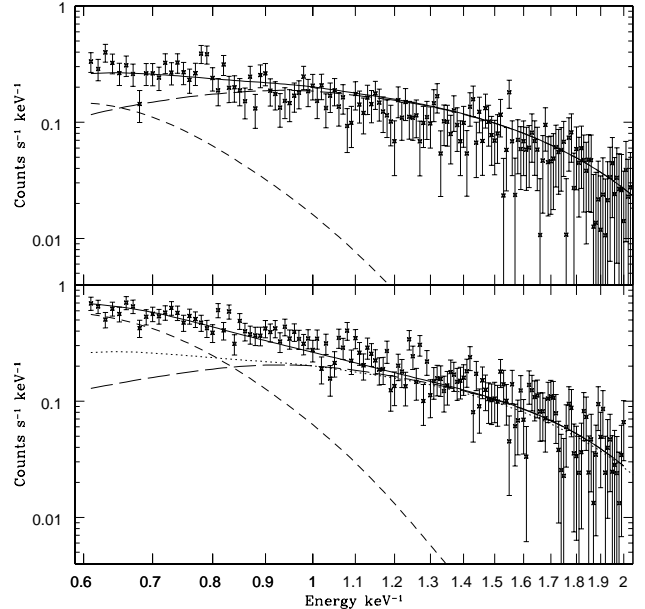


Fig. 2. *ROSAT* PSPC spectra of the SIM-selected background photons for two radio-loud quasars – PKS 0136+176 (top) and GC 1556+33 (bottom). The top spectrum fits the theoretical diffuse spectrum of Mi98 (solid line), but the same theoretical spectrum (dotted line) does not fit GC 1556+33. The best fitting spectrum (solid line) is the Mi98 spectrum with an increased emission measure of the 0.142 keV component. In both panels, the short-dashed line indicates the 0.142 keV component, and the long-dashed line the power-law component of the best-fit model.

al. 1995, Nousek et al. 1982). This also suggests that all variations in the diffuse backgrounds for the fields we examined cannot be explained, as BSH propose, by emission from clusters of galaxies, whose x-ray temperatures typically lie around a few keV rather than the 0.142 keV modeled here (see, for example, David et al. 1993).

The power-law component to the spectrum fits all of the observed fields rather well. This agrees with the conclusions of Ishisaki (1997), who found that, within systematic errors, the higher-energy diffuse x-ray background is flat on angular scales of $\sim 1^\circ$.

3. Discussion

3.1. Diffuse x-ray background level distribution

The distribution of diffuse x-ray background counts for our sample is shown in Fig. 3. The entire sample has a mean of 2606.0 ± 296.6 counts for the 10 ksec exposure, corresponding to a mean detected flux of $0.7048 \text{ photons s}^{-1} \text{ deg}^{-2}$. The distribution can be modeled by a normal distribution, shown in the figure as a solid line. A simple

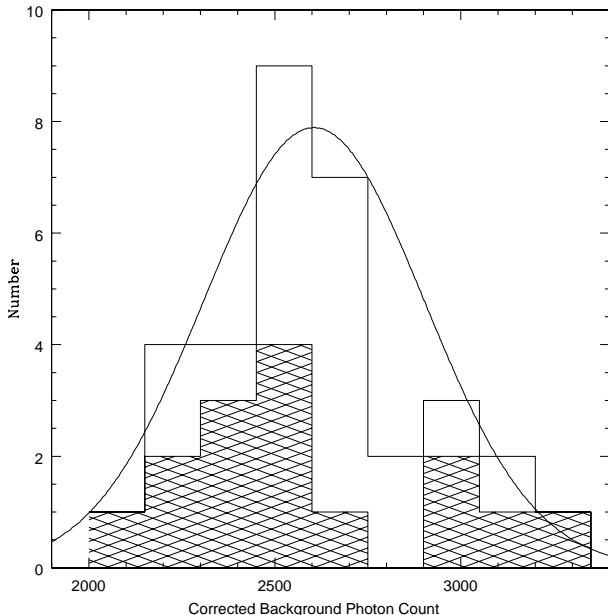


Fig. 3. A histogram of the total observed background counts for the quasar sample. The counts are corrected for N_H and represent the photons collected during a 10 050 second exposure covering $\sim 0.42 \text{ deg}^2$ of sky. The white region indicates the data for all quasars, and the hatched region indicates the data for radio-loud quasars only. The solid line indicates the Gaussian fit to the entire sample.

Kolmogorov-Smirnov (K-S) test results in a significance level of 0.957, indicating a fairly robust fit.

Examination of the radio-loud and radio-quiet quasar fields separately brings one to slightly different conclusions. The backgrounds surrounding radio-quiet quasars have a mean of 2635.5 ± 226.7 integrated counts, corresponding to a mean detected photon flux of $0.7127 \text{ photons s}^{-1} \text{ deg}^{-2}$. This is slightly higher, but not significantly so, than the mean background flux for the entire quasar sample. A K-S test comparing the radio-quiet quasars with a Gaussian distribution of the same mean and standard deviation gives a significance level of 0.953, which again indicates a rather robust fit.

The diffuse background surrounding radio-loud quasars has more ambiguous results. The radio-loud quasar background distribution is shown in Fig. 3 as the hatched histogram. At first glance, the distribution gives an indication of being bi-modal, but the small-number statistics involved means that such qualitative observations can be misleading. The diffuse x-ray backgrounds in the radio-loud quasar fields had a mean of 2570.6 ± 369.0 detected counts, corresponding to a flux of $0.6952 \text{ photons s}^{-1} \text{ deg}^{-2}$, which is slightly lower, but not significantly so, than the overall mean background population. If we try to model the radio-loud background distribution by a Gaussian, the K-S significance level is 0.363, a

level not ruling out a Gaussian fit, but not strongly supporting such a fit. Moreover, a K-S test comparing the radio-loud and radio-quiet background distributions gives only a 0.168 likelihood that the two arise from the same distribution. Again, this does not rule out that the two arise from the same distribution, but it does not support such a claim, either.

3.2. Arguments against clusters of galaxies

Due to the ambiguity of the results concerning the diffuse x-ray background surrounding radio-loud quasars, we searched for explanations supporting a two-population hypothesis. Because of the spectral analysis noted before, we consider it highly unlikely that these enhancements are due to low-luminosity x-ray clusters of galaxies as BSH suggest. Further evidence rejecting the galaxy-cluster explanation came from an analysis of the smoothness of each field once sources were removed. The remaining fluctuations in the x-ray background were not statistically significant, implying that any x-ray-emitting galaxy clusters would have to be $\gtrsim 20'$ in angular size. One would expect that galaxies in clusters of this size would be visible at optical wavelengths. A search of the $20'$ region surrounding each quasar in the NASA/IPAC Extragalactic Database (NED) revealed no known galaxy clusters which were not detected as sources and removed by the scaling-index method.

3.3. Galactic origins of enhancements

Given the apparent demise of the galaxy cluster hypothesis for the origin of the diffuse x-ray background enhancements, we need to develop another hypothesis. One likely source of large-scale x-ray emission is an extended galactic object. We located each field in the $\frac{3}{4} \text{ keV}$ -band high-resolution *ROSAT All-Sky Survey* maps of Snowden et al. (1997). Two of the radio-loud quasar fields with enhanced background emission, GC 1556+33 and PKS 1351-018, lie in regions of slightly enhanced x-ray emission due to Loop I. Also, the field surrounding 3C 216 lies in a small region of larger-scale enhanced emission. These enhancements were not obvious on the low-resolution RASS maps (Snowden et al. 1995) used in the sample selection. Therefore, it is reasonable to assert that the excess emission in these three fields is due to variations in galactic emission. The other radio-loud quasar field showing enhanced emission, 3C 454.3, does not appear to lie in regions of large-scale diffuse x-ray enhancements on the high-resolution RASS maps.

We also inspected several infrared images of the sample fields taken from the Infrared Astronomical Satellite (IRAS) data archives. A brief comparison showed no obvious connection between the diffuse x-ray background levels and infrared emission. This could suggest that our corrections for x-ray absorption were sufficient, though it also

could suggest that the observed background enhancements are not galactic in origin. The data here is too sketchy to permit a conclusion.

3.4. Possible systematic origins of enhanced background levels

We have searched for other systematics which could explain the variations in diffuse x-ray background levels. Fig. 4 shows the detected background counts as compared with observation date, galactic neutral hydrogen column densities, galactic latitudes, and quasar redshifts. The plots show no discernible correlation of background counts with these quantities, with the possible exception of observation date.

The ROSAT PSPC has been known to show variations in response with time (Prieto, Hasinger, & Snowden 1996), but these effects have been accounted for in the data reduction. A least-squares linear regression fit results in a 2σ detection of a downward trend. Such a decrease of sensitivity, on the order of 10%, would have important implications for all PSPC data reduction. The fact that no such decrement has been noticed by others casts doubt onto this hypothesis. An analysis of a much larger sample of fields, or of the same field at various epochs, would be needed to prove that a change of sensitivity with time in fact occurred.

Also shown in Fig. 4 is the cosmic x-ray background spectrum of Mi98, integrated over 10 050 ksec and folded through the ROSAT PSPC response function (solid line) and the 90% confidence limits (dashed line). This spectrum appears to underestimate the observed background. Recalling that the SIM analysis tended to give backgrounds nearly 200 counts higher than other analysis techniques brings the Mi98 spectrum into reasonable agreement with the observed background levels.

Given the discrepancies between the SIM method and more traditional source-detection routines, it is worthwhile to examine possible correlations between source fluxes and the background levels. A Spearman rank-order correlation test revealed no significant correlations between quasar flux and the background flux or between total flux of detected sources and the background flux. The same test gave a 2.29σ -likelihood of a correlation between each field's brightest-source flux and the background flux. The plot of this correlation is given in Fig. 5, and suggests that the fields with the brightest backgrounds have dimmer main sources. However, this perception is heavily biased by the lowest-flux source. Additionally, one would expect that, if the SIM were not adequately removing source photons, the brighter sources should leave a higher number of photons in the background, the opposite from what is seen. Still, this possible correlation should be kept in mind.

Despite the ambiguous statistical results, the above analysis and the spectral analysis of the variations in

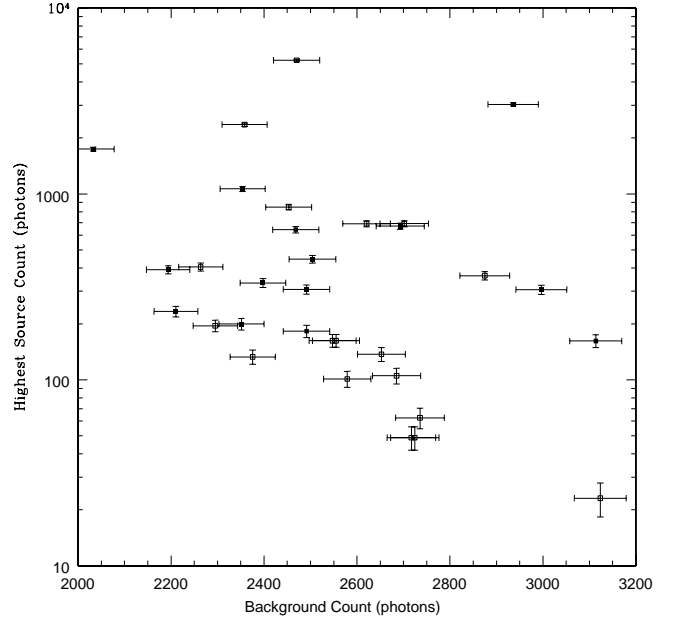


Fig. 5. The relationship between the detected counts of the brightest source in each frame is compared with the background levels. Although a Spearman rank-order correlation test gives a weak detection of a correlation (2.29σ), the large scatter (note the logarithmic scale on the vertical axis) and considerations discussed in the text cast some doubt on this detection. Error bars are the 1σ Poisson noise only. Solid blocks are for fields containing radio-quiet quasars, while open blocks indicate the fields containing radio-loud quasars.

the diffuse x-ray background surrounding quasars strongly suggests that these variations are fully explainable by variations in the hot, galactic (i.e. 0.142 keV) component of the diffuse x-ray background. The analysis also shows that there is no statistically significant difference between the diffuse x-ray backgrounds in the regions surrounding radio-loud and radio-quiet quasars.

4. Conclusions

We have examined the large-scale ($\lesssim 20'$) diffuse x-ray background surrounding 15 radio-loud and 18 radio-quiet quasars. To accomplish this, we have used a new source-detection algorithm, the scaling-index method. This method is not yet fully refined, with three major uncertainties remaining. The first of these is the lowest flux at which actual and spurious sources can be discriminated. A second concern is that the background fields so examined had higher detected x-ray emission levels than the same fields examined by other source-detection algorithms. Our final concern is that the SIM has difficulty identifying source photons in bright sources, where the photon density is highest. The SIM does offer the distinct

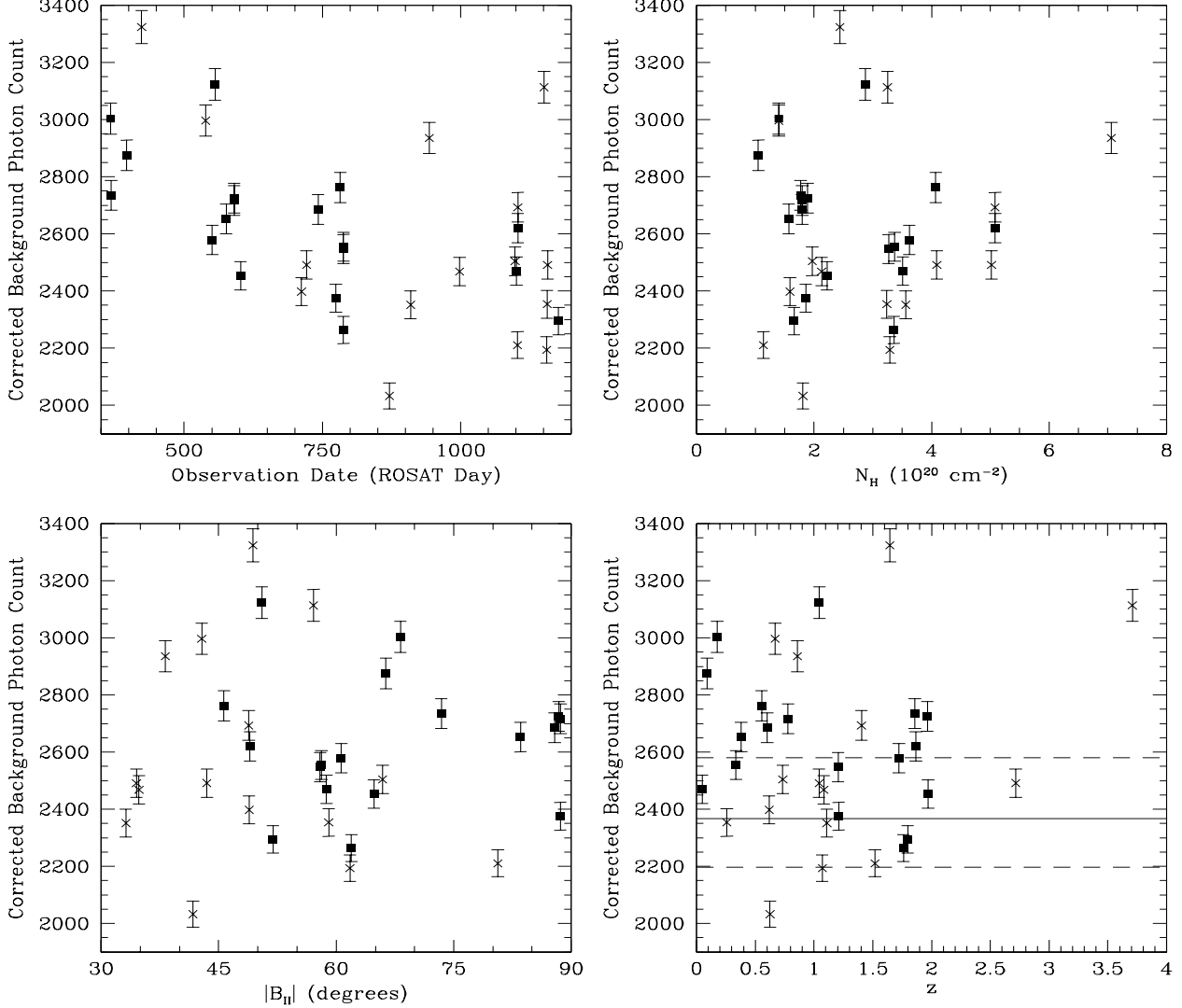


Fig. 4. Plots showing the total corrected background counts as functions of the times of observation, the galactic N_H values, the absolute value of the galactic latitude, and redshift. Filled squares represent radio-quiet quasars; crosses represent radio-loud quasars. In the plot of background counts versus redshift, the CXRB spectra as determined by Miyaji et al. (1998) and folded through the ROSAT PSPC response function is plotted. The solid line indicates best-fit values, and the dotted lines indicate the 90% errors quoted by Mi98. The error bars shown are 1σ error bars assuming Poisson photon counting statistics. No systematic errors are included.

advantage of separating background and source photons, as well as the potential to locate the true extent of extended sources.

Using the SIM, we find that the backgrounds can be adequately examined by a single Gaussian distribution with a mean of 2606.0 ± 296.6 detected photons in a 10 ksec exposure. Spectral analysis of these backgrounds suggests that the variations in the background levels is due to fluctuations in the previously-reported 0.142 keV component of the cosmic x-ray background. There is some

evidence that there may be a separate population of enhanced x-ray backgrounds surrounding some radio-loud quasars, but there is no plausible source or systematic explaining such a division. There is no evidence of large-scale diffuse emission from x-ray clusters being responsible for notable enhancement of these backgrounds, as had been hypothesized by previous analyses. Finally, we find no statistically-significant, systematic differences between the large-scale diffuse x-ray backgrounds surrounding radio-loud quasars and those surrounding radio-quiet

quasars. This suggests that x-ray evidence for differences in the local environments of quasars is either present only on angular scales of less than a few arcminutes, present only at very low flux levels, or non-existent.

Acknowledgements. The authors wish to express appreciation to M. Freyberg for helpful discussions concerning data analysis, especially in the realm of the diffuse x-ray background. Appreciation is also expressed to H. Scheingraber for discussions on the SIM. The authors also wish to thank the anonymous referee for helpful suggestions in improving this paper. KAW acknowledges the financial support of a Fulbright Fellowship from the Fulbright-Kommission, Bonn, Federal Republic of Germany and the hospitality of the MPE during his Fulbright tenure. KAW would also like to thank G.R. Penn and K. Müller-Osten for their kindness, support, and skiing lessons. This research has made use of the NASA/IPAC Extragalactic Database (NED) which is operated by the Jet Propulsion Laboratory, California Institute of Technology, under contract with the National Aeronautics and Space Administration.

References

- Bartelmann, M., Schneider, P., Hasinger, G., 1994, A&A 290, 399 (BSH)
- Boyle, B.J., Shanks, T., Yee, H.K.C., 1988, in *Large Scale Structures of the Universe, IAU Symposium No. 130*, ed. J. Audouze, M.-C. Pelletan, and A. Szalay, p. 576
- Briel, U.G., Henry, J.P., 1993, A&A 278, 379
- Burg, R., Giacconi, R., Forman, W., Jones, C., 1994, ApJ 442, 37
- David, L.P., Slyz, A., Jones, C., et al., 1993, ApJ 412, 479
- Dickey, J.M., Lockman, F.J., 1990, ARA&A 28, 215
- Fried, J.W., 1997, A&A 319, 365
- Gendreau, K.C., Mushotozky, R., Fabian, A.C., et al., 1995, PASJ 47, L5
- Grassberger, P., Badii, R., Politi, A., 1988, J. Stat. Phys. 51, 135
- Hall, P.B., Ellingson, E., Green, R.F., Yee, H.K.C., 1995, AJ 110, 513
- Ishisaki, Y., 1997, Ph.D. Thesis, University of Tokyo
- Kruskal, J.B., 1956, Proc. Am. Math. Soc. 7, 48
- Lockman, F.J., Savage, B.D., 1995, ApJS 97, 1
- McHardy, I., Jones, L., Merrifield, M., et al., 1998, MNRAS 295, 641
- Miyaji, T., Ishisaki, Y., Ogasaka, Y., et al., 1998, A&A 334, L13 (M98)
- Murphey, E.M., Lockman, F.J., Laor, A., Elvis, M., 1996, ApJS 105, 369
- Nousek, J.A., Fried, P.M., Sanders, W.T., Kraushaar, W.L., 1982, ApJ 258, 83
- Pfeffermann E., Briel U.G., Hippmann H., et al., 1986, Proc. SPIE 733, 519
- Prieto, M.A., Hasinger, G., Snowden, S.L., 1996, A&AS 120, 187
- Prim, R.C., 1957, Bell Syst. Tech. J. 36, 1389
- Snowden, S.L., Freyberg, M.J., Plucinsky, P.P., et al., 1995, ApJ 454, 643
- Snowden, S.L., Egger, R., Freyberg, M.J., et al., 1997, ApJ 485, 125
- Véron-Cetty, M.P., Véron, P., 1993, ESO Scientific Report 13
- Voges, W., Boller, Th., Dennerl, K., et al., 1996, in *Röntgenstrahlung from the Universe*, ed. H.U. Zimmermann, J. Trümper, and H. Yorke, MPE Report 263, p.637
- Wiedenmann, G., Scheingraber, H., Voges, W., 1997, in *Data Analysis in Astronomy*, ed. V Di Gesù, M.J.B. Duff, A. Heck, et al. (Singapore: World Scientific) (WSV)
- Zimmermann, H.U., Belloni, T., Boese, G., et al., 1992, in *Data Analysis in Astronomy IV*, ed. V. Di Gesù, L. Scarsi, R. Bucchini, et al., p.141 (New York: Plenum Press)